

Effect of uncertainties in geometry, inter-layer boundary and shear strength properties on the probabilistic stability of a 3D embankment slope

Varkey, Divya; Hicks, Michael A.; Vardon, Philip J.

DOI

[10.1080/17499518.2022.2101066](https://doi.org/10.1080/17499518.2022.2101066)

Publication date

2022

Document Version

Final published version

Published in

Georisk

Citation (APA)

Varkey, D., Hicks, M. A., & Vardon, P. J. (2022). Effect of uncertainties in geometry, inter-layer boundary and shear strength properties on the probabilistic stability of a 3D embankment slope. *Georisk*, 17(2), 262-276. <https://doi.org/10.1080/17499518.2022.2101066>

Important note

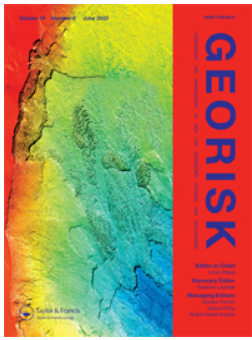
To cite this publication, please use the final published version (if applicable). Please check the document version above.

Copyright

Other than for strictly personal use, it is not permitted to download, forward or distribute the text or part of it, without the consent of the author(s) and/or copyright holder(s), unless the work is under an open content license such as Creative Commons.

Takedown policy

Please contact us and provide details if you believe this document breaches copyrights. We will remove access to the work immediately and investigate your claim.



Georisk: Assessment and Management of Risk for Engineered Systems and Geohazards

ISSN: (Print) (Online) Journal homepage: <https://www.tandfonline.com/loi/ngrk20>

Effect of uncertainties in geometry, inter-layer boundary and shear strength properties on the probabilistic stability of a 3D embankment slope

Divya Varkey, Michael A. Hicks & Philip J. Vardon

To cite this article: Divya Varkey, Michael A. Hicks & Philip J. Vardon (2022): Effect of uncertainties in geometry, inter-layer boundary and shear strength properties on the probabilistic stability of a 3D embankment slope, Georisk: Assessment and Management of Risk for Engineered Systems and Geohazards, DOI: [10.1080/17499518.2022.2101066](https://doi.org/10.1080/17499518.2022.2101066)

To link to this article: <https://doi.org/10.1080/17499518.2022.2101066>



© 2022 The Author(s). Published by Informa UK Limited, trading as Taylor & Francis Group



Published online: 11 Aug 2022.



Submit your article to this journal [↗](#)



Article views: 208



View related articles [↗](#)



View Crossmark data [↗](#)

Effect of uncertainties in geometry, inter-layer boundary and shear strength properties on the probabilistic stability of a 3D embankment slope

Divya Varkey, Michael A. Hicks  and Philip J. Vardon

Section of Geo-Engineering, Faculty of Civil Engineering and Geosciences, Delft University of Technology, The Netherlands

ABSTRACT

This paper investigates the influence of three forms of uncertainty on the probabilistic stability of an idealised 3D embankment slope. These are: 1D spatial variability in the external geometry of the slope along its length, 2D spatial variability in the depth of the boundary between the embankment material and the foundation layer, and 3D spatial variability in the shear strength properties of the slope and foundation materials. The relative influence of each uncertainty has been investigated using the random finite element method, based on statistics consistent with a Dutch regional dyke. The results indicate that, for such a structure, the soil spatial variability has a much greater influence than uncertainties relating to embankment geometry and inter-layer boundary. In particular, it is demonstrated that the spatial correlation of material properties along the length of the embankment has a greater influence on the probabilistic characteristics of the embankment slope stability and failure consequence than the spatial correlation of properties perpendicular to it. A worst case scale of fluctuation for the material properties is identified.

ARTICLE HISTORY

Received 17 March 2021
Accepted 8 July 2022

KEYWORDS

Geometry; random finite element method; slope stability; spatial variability; three dimensional



1. Introduction

A numerical model is an idealised representation of the complex reality of a problem and hence uncertainties are always present. There are three main sources of uncertainty in the material parameters: measurement uncertainty, transformation uncertainty and inherent spatial variability of the properties arising due to a combination of physical, chemical and depositional processes (Phoon and Kulhawy 1999). Much research, especially in 2D, has been done on the influence of spatial variability of the material properties by utilising various modelling techniques, including the random finite element method (RFEM) (Fenton and Griffiths 2008) which combines random fields of soil properties with finite elements. For example, Hicks and Samy (2002, 2004), Griffiths and Fenton (2004), Hicks and Onisiphorou (2005), Griffiths, Huang, and Fenton (2009a), Huang et al. (2010) and Javankhoshdel, Luo, and Bathurst (2017) used RFEM to investigate the influence of heterogeneity in soil shear strength on the stability of 2D slopes; Vardon, Liu, and Hicks (2016) used inverse analysis to reduce the spatial uncertainty in hydraulic conductivity and shear strength parameters in the RFEM analysis of a 2D slope; and Johari and

Gholampour (2018) used conditional random fields for the reliability-based stability assessment of slopes in unsaturated soils.

A challenging task in the uncertainty modelling is estimating the scale of fluctuation of the material properties (i.e. the length over which the property values are significantly correlated) as it often requires a large number of CPTs to be placed strategically (Lloret-Cabot, Fenton, and Hicks 2014; Ching et al. 2018; de Gast, Vardon, and Hicks 2021). Therefore, it is rarely possible to obtain reliable estimates of the scales of fluctuation in practice, although values typically in the range of 0.3–3 m in the vertical direction and 10–40 m in the horizontal direction are suggested in the literature. El-Ramly, Morgenstern, and Cruden (2003) carried out a detailed literature review of the scales of fluctuation reported for different soil types, properties and testing methods and found that the reported values were not very different from each other.

Hicks et al. (2019) illustrated the advantage of incorporating spatial variability of soil properties, by using RFEM for the reliability-based stability assessment of a regional dyke in the Netherlands and comparing the results with those from a much simpler approach

CONTACT Michael A. Hicks  m.a.hicks@tudelft.nl  Technische Universiteit Delft, Faculteit Civiele Techniek en Geowetenschappen, 2600 GA Delft, Netherlands

© 2022 The Author(s). Published by Informa UK Limited, trading as Taylor & Francis Group
This is an Open Access article distributed under the terms of the Creative Commons Attribution-NonCommercial-NoDerivatives License (<http://creativecommons.org/licenses/by-nc-nd/4.0/>), which permits non-commercial re-use, distribution, and reproduction in any medium, provided the original work is properly cited, and is not altered, transformed, or built upon in any way.

based on characteristic soil properties. For the same dyke cross-section, Varkey et al. (2020) compared factors of safety obtained using characteristic values derived using various analytical equations with the factors of safety computed directly using RFEM, and thereby demonstrated the reduction in over-conservatism possible when using RFEM. However, only a limited amount of research (Griffiths, Huang, and Fenton 2009b; Hicks and Spencer 2010; Huang et al. 2013; Hicks, Nuttall, and Chen 2014; Ji and Chan 2014; Hicks and Li 2018; Varkey, Hicks, and Vardon 2019) has been done on the influence of 3D spatial variability of soil properties in the reliability-based assessment of slopes, especially using RFEM, owing to the large computational requirements. Moreover, researchers have previously conducted 3D reliability-based assessments assuming the same scale of fluctuation of the shear strength properties for all directions in the horizontal plane. However, a detailed investigation of horizontal scales of fluctuation below a Dutch regional dyke (de Gast, Vardon, and Hicks 2019, 2021) revealed the scale of fluctuation along the dyke to be higher than across the dyke.

An additional idealisation typical in 3D embankment analyses has been to consider the slope geometry to be deterministic for assumed ‘uniform’ sections in the longitudinal direction, although it is observed in practice that variations in geometry do occur along the length of a dyke. However, Juang et al. (2019) recently looked at variations in the height of an infinite slope combined with variations in the shear strength properties and observed that the variations in geometry had a less significant impact on slope reliability than the latter for the problem they analysed.

In recent years, the uncertainty arising due to stratigraphic heterogeneity of materials layers, i.e. the uncertainty in determining the exact location of different layers at unsampled locations, has received increasing attention. For modelling stratigraphic uncertainty, two approaches have been widely adopted: (i) a boundary-based model (Li, Zhang, and Li 2016) which assumes a continuous function to define the spatial correlation in the location (i.e. depth) of the boundary separating two materials; and (ii) a category-based model (Qi et al. 2016) which predicts finite and discrete material categories using a coupled Markov chain method (Elfeki and Dekking 2001). Xiao et al. (2017) compared the pros and cons of the two approaches and developed a 2D heuristic approach combining both models. They observed that the category-based model was a better approach to model the natural weathering process and complicated anisotropic material transitions in 2D, whereas the boundary-based model was suggested to

be more suitable for uniformly stratified cases. It was also observed that the boundary-based model can incorporate material spatial variability and can easily be extended to the modelling of 3D stratigraphic uncertainty (Li et al. 2016), whereas extending the category-based model to 3D stratigraphic uncertainty modelling is rather difficult (Liang, Wang, and Guo 2014). Deng et al. (2017) evaluated the reliability of a slope considering 2D soil spatial variability and stratigraphic uncertainty using the category-based model. They observed that the location, layout and number of boreholes had a significant influence on the reliability of the slope. Recently, Wang et al. (2019) introduced a clustering-based approach to identify subsurface stratification using CPT and borehole data. Meanwhile, Zhao and Wang (2020) proposed an interpolation technique for characterising multilayer soil property profiles from sparse measurements, in conjunction with the clustering-based approach for soil stratification.

In this paper, the authors investigate the influence of three forms of uncertainty on the probabilistic stability of a 3D embankment slope, based on statistics consistent with a Dutch regional dyke (Hicks et al. 2019; de Gast et al. 2021; de Gast, Vardon, and Hicks 2021). These are due to anisotropic spatial variability of the shear strength parameters, spatial variability in the geometry of the slope along its length, and spatial variability in the depth of the boundary separating the slope and foundation materials. These uncertainties have been modelled by random fields, as they are assumed to be stationary stochastic processes which can be defined by a trend and a variation with zero mean (Rackwitz 2000), and linked with the finite element method within a Monte-Carlo framework.

2. Description of the example problem

Figure 1 shows an idealised 45° slope, 5 m high (H) and 50 m long (L), resting on a 4 m deep foundation

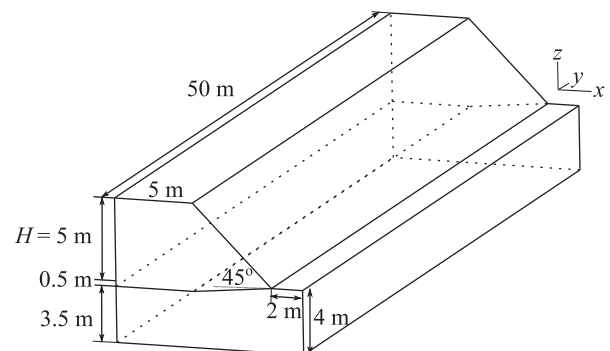


Figure 1. Geometry of the problem

Table 1. Soil parameter values

Parameter	Mean value	COV	θ_z	θ_x and θ_y
Cohesion (c')	10 kPa for slope and 8 kPa for foundation	0.2	1 m	1–2000 m
Friction angle (φ')	25° for slope and 20° for foundation	0.2	1 m	1–2000 m
Dilation angle	0°	0.0	–	–
Young's modulus	10 ⁵ kPa	0.0	–	–
Poisson's ratio	0.3	0.0	–	–
Unit weight	20 kN/m ³	0.0	–	–

layer, which has been used in this paper as an example. A foundation settlement of 0.5 m has been assumed under the crest of the slope to account for compression of the subsoil due to the weight of the embankment, and this reduces linearly under the sloping face of the embankment to 0 m at the toe. The slope and foundation layer were meshed with a total of 8800, 20-node, regular hexahedral elements of approximate size 0.5 m in depth and 1 m×1 m in plan, and using a 2×2×2 Gaussian integration scheme. This discretisation was chosen to ensure adequate characterisation of the spatial variability for the smallest scale of fluctuation considered (Spencer 2007). The mesh was fixed at the base, whereas 2D rollers on the y - z faces prevented movement in the x direction and 1D rollers on the x - z faces allowed movement only in the z direction (see Spencer (2007) and Hicks and Li (2018) for an explanation and validation of these boundary conditions, which were implemented to prevent a tendency for failure mechanisms to be attracted to the mesh ends). The soil parameters are summarised in Table 1. A coefficient of variation (COV) of 0.2 was used for the shear strength parameters (cohesion c' and friction angle φ') of both the slope and foundation, which is within the typical range of values (Phoon and Kulhawy 1999; Cherubini 2000), and the other parameters were considered to be deterministic. A vertical scale of fluctuation of 1 m (see, for example, Hicks et al. (2019), de Gast et al. (2021) and de Gast, Vardon, and Hicks 2021) and a range of values for the horizontal scale of fluctuation of c' and φ' have been considered to generate the random fields. In this study, c' and φ' were assumed to be uncorrelated.

3. Modelling strategy

The spatial variability of properties is mathematically represented using random fields, with an ensemble of random fields being used to represent the uncertainty in the spatial distribution. Each realisation (random field) is based on the same underlying statistics, but each will be different with respect to the spatial distribution of property values. In this paper, the continuous random fields have been discretised as spatial averages

using the Local Average Subdivision (LAS) method (Fenton and Vanmarcke 1990). Following generation over a large cuboidal domain and transformation to the physical space, the random field (cell) values from a randomly selected section of the larger domain are mapped to the finite elements at the Gauss point level and the boundary-value problem then analysed within a Monte Carlo framework using RFEM. The generation of random fields and the finite element slope stability analyses have been carried out using an in-house computer code incorporating a direct (global) solver (see, for example, Spencer (2007), Hicks and Spencer (2010), Hicks, Nuttall, and Chen (2014) and Hicks and Li (2018)). The strength reduction method has here been used to compute the factor of safety of the slope in each realisation of the Monte Carlo simulation. In this method, gravity loading is applied to generate the in-situ stresses. The resulting shear stresses are checked against the Mohr-Coulomb failure criterion and excess stresses are iteratively redistributed throughout the model. If equilibrium is achieved within 500 iterations, the shear strength parameters are reduced in a subsequent step and the whole process is repeated. The lowest strength reduction factor to trigger failure (as indicated by no equilibrium convergence) is the factor of safety F of the slope for that realisation. A total of 500 Monte Carlo simulations have been carried out for each RFEM analysis presented in this paper, which was found to be sufficient to ensure convergence of the output statistics (i.e. mean and standard deviation of F) for the problem analysed (see Spencer (2007), Li, Hicks, and Nuttall (2015), Li (2017) and Hicks and Li (2018) for illustrations of the convergence of the mean and standard deviation of F for similar slope stability problems). However, for those applications in which small probabilities of failure need to be accurately computed, more advanced techniques such as subset simulation may be employed to keep the required number of simulations to an acceptable level (van den Eijnden and Hicks 2017).

The point and spatial statistics of the various parameters considered below are listed in Tables 1 and 2. Because of the relatively low values assumed for the COVs of the parameters in the tables, normal distributions have been considered adequate for modelling

Table 2. Statistics of geometric and boundary parameters: (a) geometric uncertainty; (b) inter-layer boundary uncertainty

(a)					
Parameter	Mean (m)	COV	θ_y (m)	Resulting range of values (m)	
Slope height H	5	0.03	10	4.55–5.45	
Toe width T	10	0.03	10	9.10–10.90	
Crest width C	5	0.03	10	4.55–5.45	
(b)					
Location (relative to toe)	Mean (m)	COV	θ_x (m)	θ_y (m)	Resulting range of values (m)
Under the crest (linearly decreasing to 0 m at the toe)	5	0.03	10	10	4.55–5.45

parameter uncertainty, since, for $COV < 0.33$, there is negligible influence of truncating distributions to prevent negative values.

3.1. Modelling of geometric uncertainty

Uncertainty in the form of different cross-sectional geometries along the slope length are considered in this paper. Specifically, uncertainty in the various cross-sectional parameters of the slope, that is, height H , crest width C and toe width T , have been modelled as 1D random fields using the correlation function:

$$\rho(\tau_y) = \exp\left(-\frac{2\tau_y}{\theta_y}\right) \quad (1)$$

where τ_y is the lag distance and θ_y is the scale of fluctuation in the y direction.

Depending on the generated field values, in each realisation the nodes of the finite element mesh are moved in the x - z plane to generate different cross-sectional geometries in the slope length (y) direction. As illustrated in Figure 2, based on the generated field value for H at a certain location y , all nodes (of the slope, but not the foundation layer) in the x - z plane corresponding to the y -location are moved in the z direction. Similarly, based on the generated field values for the crest and toe widths at each location y , all nodes in the x - z plane (in the slope and foundation layer) are translated in the x direction.

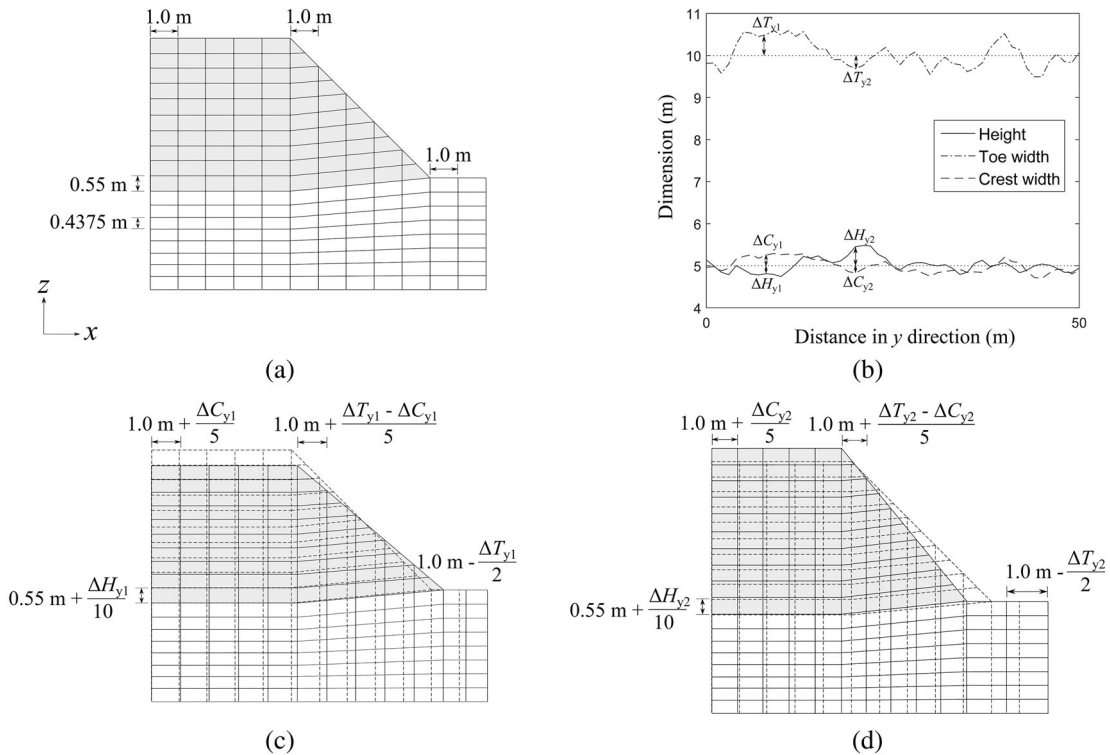


Figure 2. Generation of different cross-sections along the slope length: (a) original (reference) cross-section; (b) typical 1D random fields for slope height (H), toe width (T) and crest width (C) along the slope length; (c) cross-section generated at $y = y_1$ (shown by solid lines); (d) cross-section generated at $y = y_2$ (shown by solid lines)

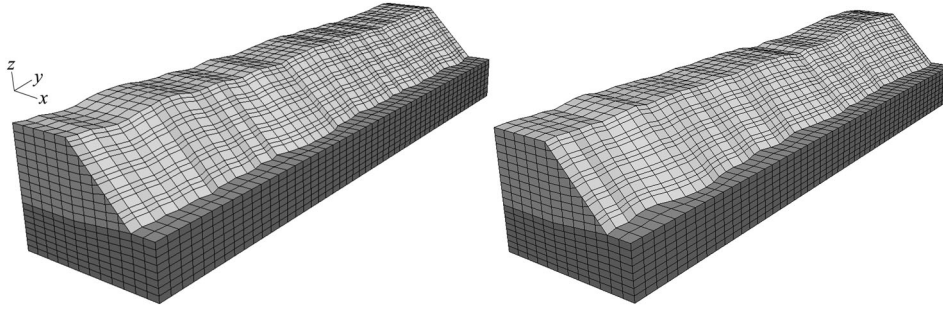


Figure 3. Typical mesh realisations considering geometric uncertainty

The point statistics of the normal distributions defining the uncertainties in the geometric parameters were chosen to give a range of possible values up to around 10% (i.e. ± 3 standard deviations) either side of the mean (see Table 2a), which is on the conservative side based on the fluctuations generally found for Dutch regional dykes. The variations in the crest and toe widths were correlated using the following equation:

$$\boldsymbol{\xi} = \mathbf{L}\mathbf{Z} \quad (2)$$

$$\mathbf{L}\mathbf{L}^T = \mathbf{R} = \begin{bmatrix} 1 & \rho_{z_1 z_2} & \cdots & \rho_{z_1 z_n} \\ \rho_{z_2 z_1} & 1 & \cdots & \rho_{z_2 z_n} \\ \cdots & \cdots & \cdots & \cdots \\ \rho_{z_n z_1} & \rho_{z_n z_2} & \cdots & 1 \end{bmatrix} \quad (3)$$

where \mathbf{L} is the lower triangular matrix obtained by the decomposition of the correlation matrix \mathbf{R} (Equation (3)), $\rho_{z_i z_j}$ is the Pearson cross-correlation coefficient between the random variables Z_i and Z_j , and $\boldsymbol{\xi}$ and \mathbf{Z} are the vectors of correlated and uncorrelated standard normal random variables of size n . A value of 0.75 has been adopted for the cross-correlation coefficient between the crest and toe widths, to reflect that a wider crest is likely to be associated with an embankment that is wider at the base, whereas variations in H have been taken as uncorrelated with respect to these quantities. Note that, as a result of the variations in H , crest width and toe width, variations of up to $\pm 5^\circ$ in the slope angle have been generated, which are likely to be on the conservative side based on ground surface measurements of a regional dyke in the Netherlands (de Gast 2020). Figure 3 illustrates the meshes generated in two realisations.

3.2. Modelling of inter-layer boundary uncertainty

To model the uncertainty in the location of the boundary between the embankment and the underlying foundation layer (which may, for example, have arisen due to

the spatially variable compression of underlying soft soils), a 2D random field has been used with the following correlation function:

$$\rho(\tau_x, \tau_y) = \exp\left(-\sqrt{\left(\frac{2\tau_x}{\theta_x}\right)^2 + \left(\frac{2\tau_y}{\theta_y}\right)^2}\right) \quad (4)$$

where τ_x and τ_y are the lag distances and θ_x and θ_y are the scales of fluctuation in the x and y directions, respectively.

The point statistics of the normal distribution defining this uncertainty are listed in Table 2b. An isotropic horizontal correlation length of 10 m has been assumed for the boundary uncertainty, unless stated otherwise. Based on the field value at an x - y location corresponding to a column of nodes in the finite element mesh, the locations of all nodes of the finite element mesh, above and below the boundary, are adjusted vertically. Figure 4 illustrates the depth profiles of the boundary generated in two realisations. When considering this form of uncertainty alone, the external geometry remains constant; that is, although the effective height of the embankment varies with respect to the inter-layer boundary, the external height is unaffected (as is indicated in Figure 4).

3.3. Modelling of anisotropic material uncertainty

The spatial uncertainty in material properties is modelled using 3D random fields generated using the following 3D separable Gauss Markov correlation function:

$$\rho(\tau_x, \tau_y, \tau_z) = \exp\left(-\frac{2\tau_z}{\theta_z} - \sqrt{\left(\frac{2\tau_x}{\theta_x}\right)^2 + \left(\frac{2\tau_y}{\theta_y}\right)^2}\right) \quad (5)$$

where τ_x , τ_y and τ_z are the lag distances and θ_x , θ_y and θ_z are the scales of fluctuation in the respective directions. The separation of the vertical (z) correlation structure

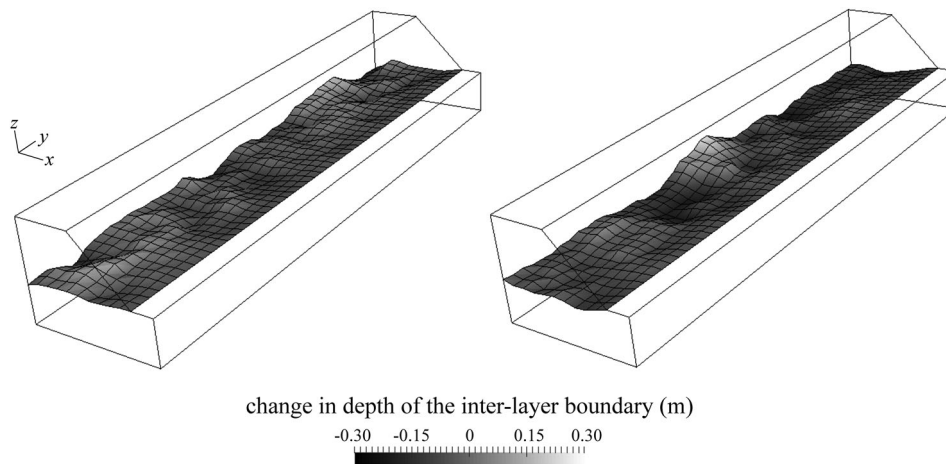


Figure 4. Typical realisations of inter-layer boundary depth profiles (variations scaled-up by a factor of 5 for better visualisation)

from the two horizontal (x and y) directions was done to model the long-term depositional characteristic in the soil.

The method of random field generation follows Hicks and Spencer (2010) and Li (2017). It begins with generating isotropic standard normal fields, i.e. with $\theta_x = \theta_y = \theta_z$ in Equation (5), followed by transformation to anisotropic standard normal fields. This is carried out by squashing and/or stretching the isotropic fields in the required directions. The generated standard normal fields are then transformed to their physical space and mapped to the Gauss points of the finite element mesh. Figure 5 illustrates typical random fields of c' mapped to an idealised 3D slope.

4. Results and discussions

A deterministic analysis of the slope using the mean parameters listed in Tables 1 and 2 resulted in a factor of safety of $F = 1.395$. Figure 6 shows the histogram of F obtained by analysing the slope accounting only for uncertainties in the material parameters, and using $\theta_x = \theta_y = 10$ m and $\theta_z = 1$ m. As shown in the figure, the mean F from the stochastic analysis is lower than the deterministic F (shown as a dashed line), due to the greater influence of weaker zones on slope failure in a heterogeneous soil. The results obtained by analysing the slope with uncertainties in the material properties, as well as with uncertainties in the geometry and/

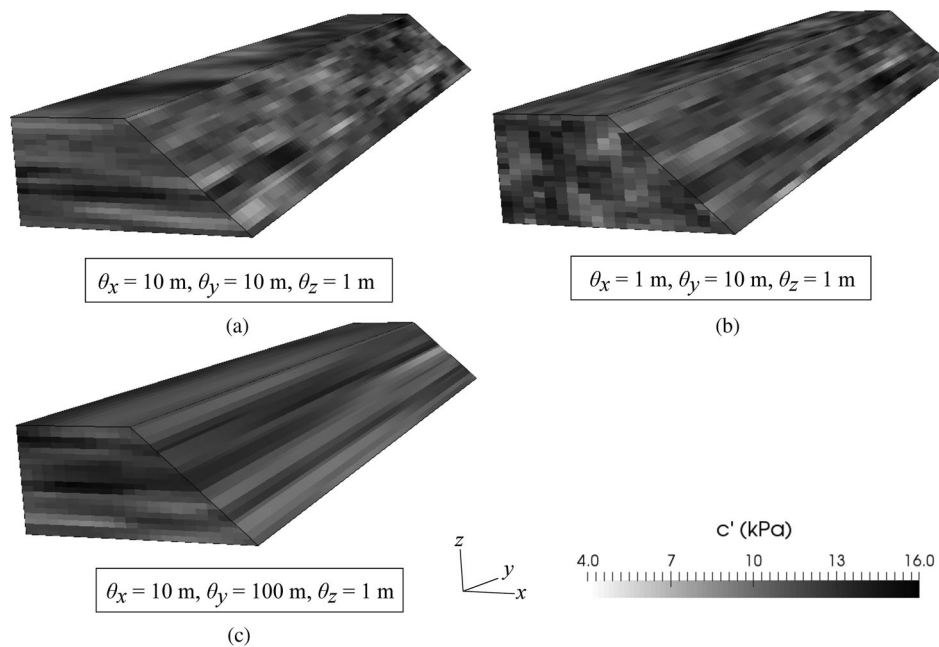


Figure 5. Typical realisations of c' generated from isotropic 3D random fields with $\theta = 10$ m, by: (a) squashing in the z direction, (b) squashing in the x and z directions, and (c) stretching in the y and squashing in the z directions

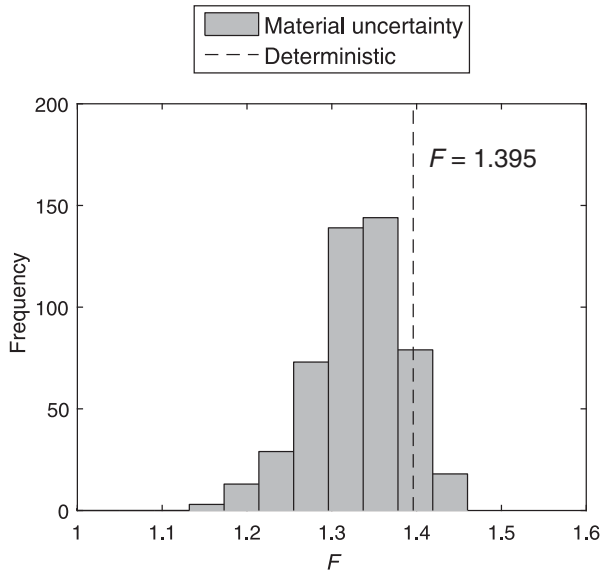


Figure 6. Histogram of F obtained based on material uncertainty, compared with the deterministic solution

or boundary between the slope and foundation layer, are discussed below. The histograms of F , obtained by considering the uncertainties in the various input variables, were approximated by normal distributions in order to obtain cumulative distributions (cdf) of F .

4.1. Influence of 1D geometric uncertainty

The cdf of F obtained by analysing the slope with uncertainty only in the external geometry, as defined by the

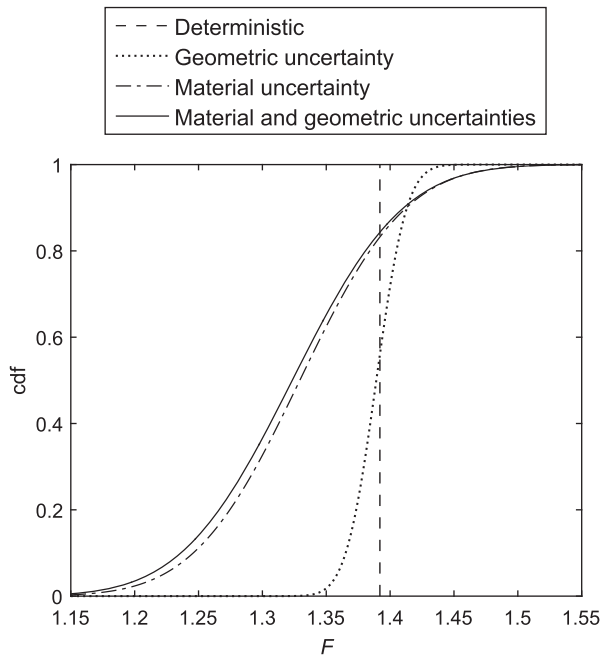


Figure 7. Cdfs of F obtained with geometric and material uncertainties

point statistics and θ_y in Table 2a, is shown in Figure 7. Also shown in the figure are the cdf of F obtained by considering uncertainty only in the material properties with $\theta_x = \theta_y = 10$ m and $\theta_z = 1$ m, and that obtained by considering the geometric and material uncertainties together. The distribution of F obtained by considering only the geometric uncertainty is centred near the deterministic $F = 1.395$ based on the mean parameter values, whereas those which include uncertainty in the material properties are shifted to the left due to the presence of weaker zones attracting failure.

Figure 8 illustrates the relative impact of each uncertainty on the performance of the slope. Figure 8a compares the F obtained by considering the two uncertainties together, with the F obtained for the same realisation by considering only the geometric uncertainty. Similarly, Figure 8b compares the F obtained by considering the two uncertainties with the F obtained in the same realisation by considering only

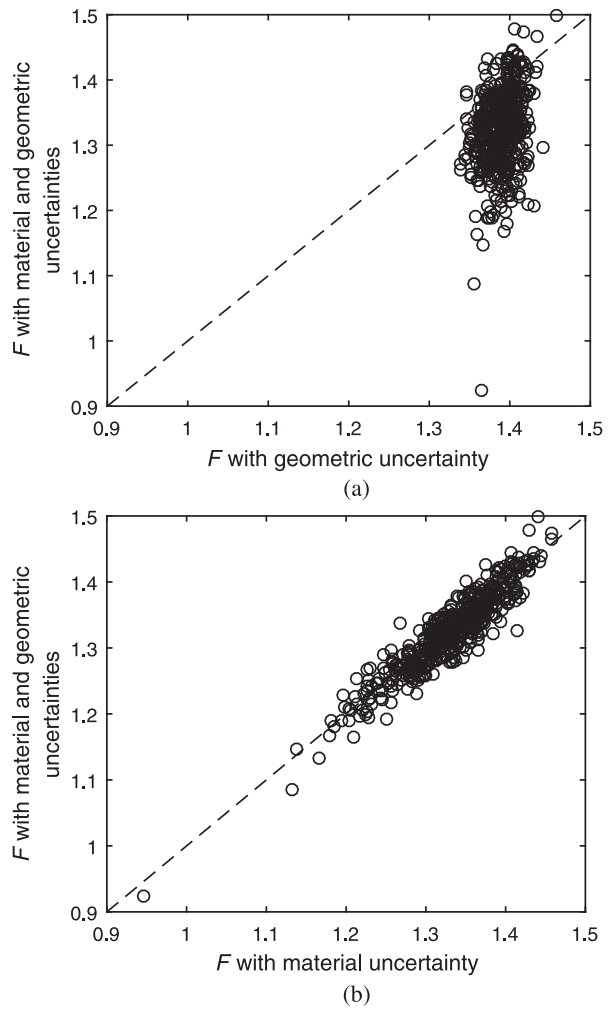


Figure 8. Comparing F obtained based on the material and geometric uncertainties, with F obtained in the same realisations based only on (a) geometric and (b) material uncertainties

the material uncertainty. The points are aligned along the dashed 1:1 line in Figure 8b, whereas no definite correlation can be derived from the points in Figure 8a. Figures 7 and 8 clearly indicate the relatively small influence of the geometric uncertainty compared to the material uncertainty.

Thus, for the COVs of parameters considered in this paper, which are within the range reported in literature for material uncertainty and consistent with the maximum variations generally expected in geometry for a regional dyke, the results indicate the larger relative influence of the spatial variability in the material properties. However, this inference may be restricted to the specific (simplified) problem considered in this paper and further research may be warranted to arrive at a firm conclusion regarding the relative importance of the two uncertainties. For that purpose, remote sensing data could be used to provide more information on the variation in external geometry. However, the frequency of the fluctuations in external geometric parameters considered in this paper is likely to be on the high side (i.e. $\theta_y = 10$ m is probably an underestimate, based on the visual inspection of Dutch regional dykes), thereby resulting in a conservative influence on the distribution of F .

4.2. Influence of 2D boundary uncertainty

The cdfs of F obtained by analysing the slope with uncertainty in the location of the boundary between the layers (i.e. between the slope material and the foundation layer) are shown in Figure 9. A range of values for the isotropic spatial variability ($\theta_x = \theta_y$) of the uncertainty in the boundary location have been considered in

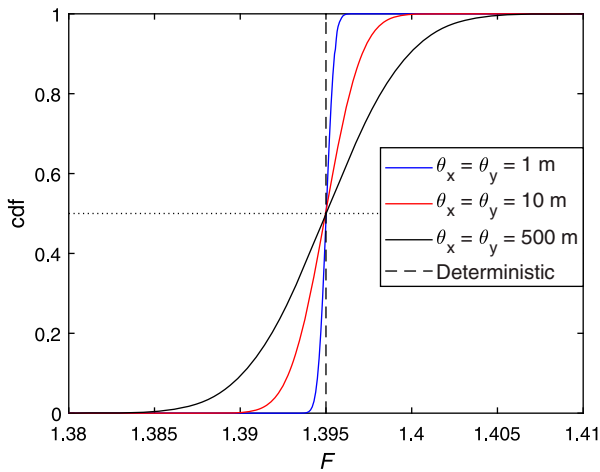


Figure 9. Cdfs of F obtained with various scales of fluctuation in the inter-layer boundary uncertainty, compared with the deterministic solution

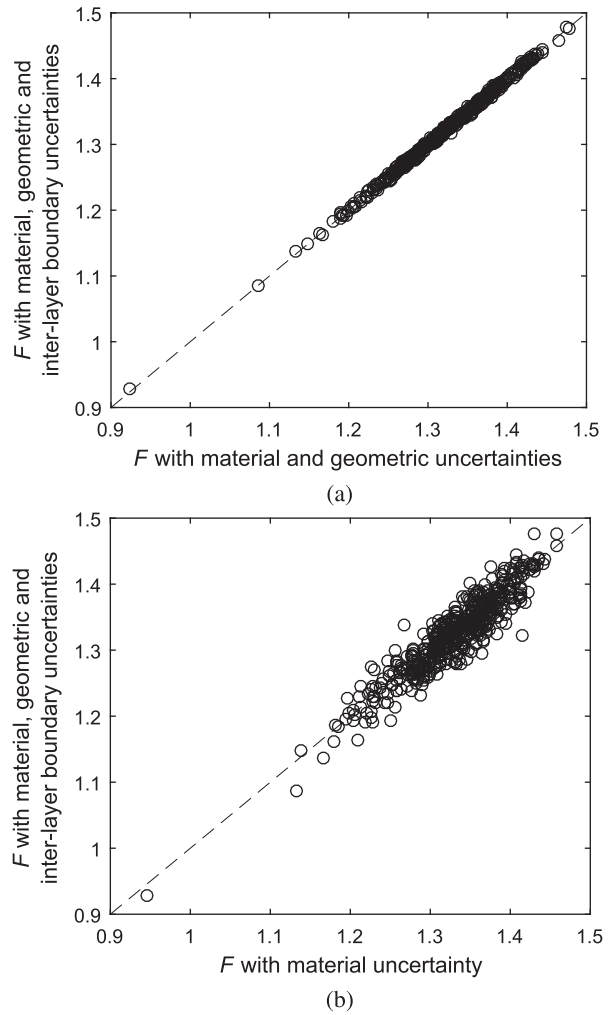


Figure 10. Comparing F obtained based on the material, geometric and inter-layer boundary uncertainties, with F obtained in the same realisations based on (a) material and geometric uncertainties, and (b) only material uncertainty

the analyses. As shown in the figure, a very small correlation length results in a narrower distribution of F compared with larger correlation lengths, although the means of the distributions are the same as the deterministic F ($= 1.395$). Moreover, a comparison of the range of responses in Figure 9 to those in Figure 7 indicates the very small influence of the boundary uncertainty on the probabilistic characteristics of the slope stability with respect to influences due to the geometric and/or material uncertainties.

To illustrate the above, Figure 10a compares the F obtained by considering all three uncertainties (material, geometric and boundary) with those obtained in the same realisations considering only uncertainties in the geometric and material properties. Similarly, Figure 10b compares the F obtained by considering all three uncertainties together with those obtained in the same realisations with only the material uncertainty.

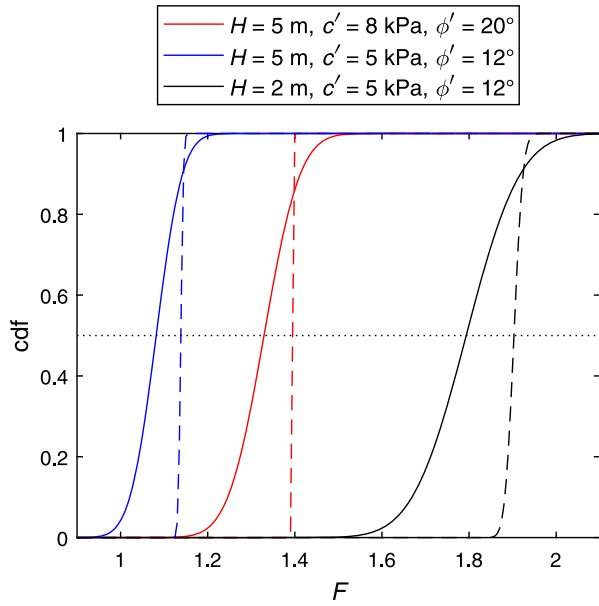


Figure 11. Cdfs of F obtained with various values of H and various mean shear strength properties for the foundation material; solid curves are based only on material uncertainty and dashed curves are based only on inter-layer boundary uncertainty

These plots are based on the spatial statistics given in Table 2 for the geometric and boundary uncertainties, and on $\theta_x = \theta_y = 10$ m and $\theta_z = 1$ m for the material uncertainty. Figure 10 shows that the points are aligned along the 1:1 line (with the points in Figure 10a having far less scatter than those in Figure 10b). These results further demonstrate the significant influence of the material uncertainty on F , as well as the negligible influence of the boundary uncertainty.

However, the above inference could be dependent on the relative shear strength properties in the two layers and on the geometry of the problem itself. Hence, further analyses were carried out with different slope geometries and with different mean c' and mean ϕ' for the foundation material. The cdfs of F obtained in the various cases are shown in Figure 11. It is clear that the responses of the slopes are significantly influenced by the material uncertainty, whereas the inter-layer boundary uncertainty has a minor or negligible influence. For the various cases considered here, the point statistics defining the uncertainty in the slope material and the boundary between the layers are the same as in Table 1 and Table 2b, respectively, and the COV of the shear strength parameters for the foundation material is fixed at 0.20.

Note that, since the geometric and boundary uncertainties have been modelled by distorting the elements in the finite element mesh (see Sections 3.1 and 3.2), this modelling approach will also distort

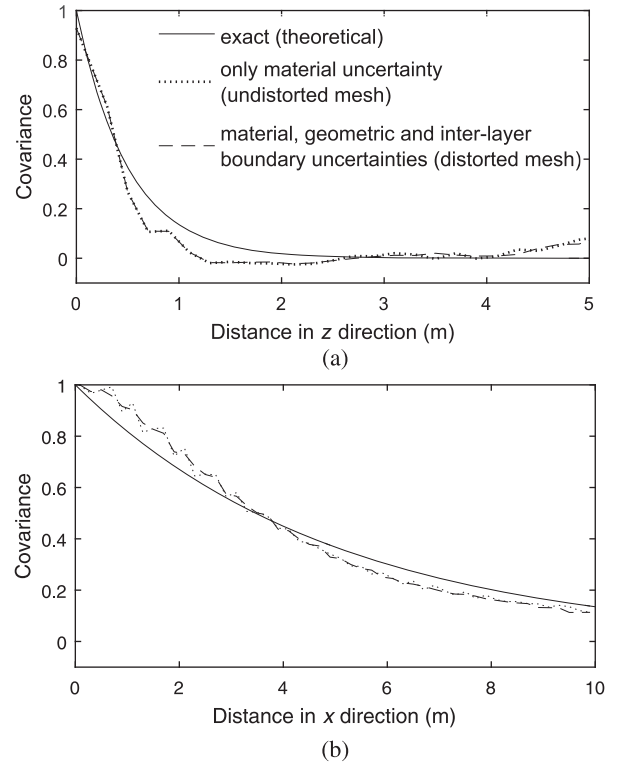


Figure 12. Covariances back-calculated from the standard normal 3D random fields of material properties, in (a) the vertical (z) direction (with $\theta_z = 1$ m), and (b) the horizontal (x) direction (with $\theta_x = 10$ m)

(to some extent) the spatial correlation structure of the material properties, as the material correlation structure is modelled relative to an undistorted mesh. Figure 12 shows covariances of the standard normal random fields of the material properties averaged over 500 realisations, as well as the exact covariances in the respective directions. For each realisation, the covariance (C) was calculated using the following equation:

$$C_{j,k} = \frac{1}{n-1} \sum_{i=1}^{n-j} (Z_i \times Z_{i+j}) \quad (6)$$

where n is the number of cell values considered in the k direction, and Z_i and Z_{i+j} are the standard normal values at cell locations i and $i+j$ in the k direction. The exact covariance in each direction was calculated using Equation (5), by using only the associated terms in that direction. Figure 12 shows that the calculated covariances agree well with the expected covariances in the respective directions, illustrating that the spatial correlation structures of the material properties were preserved despite the distorted mesh.

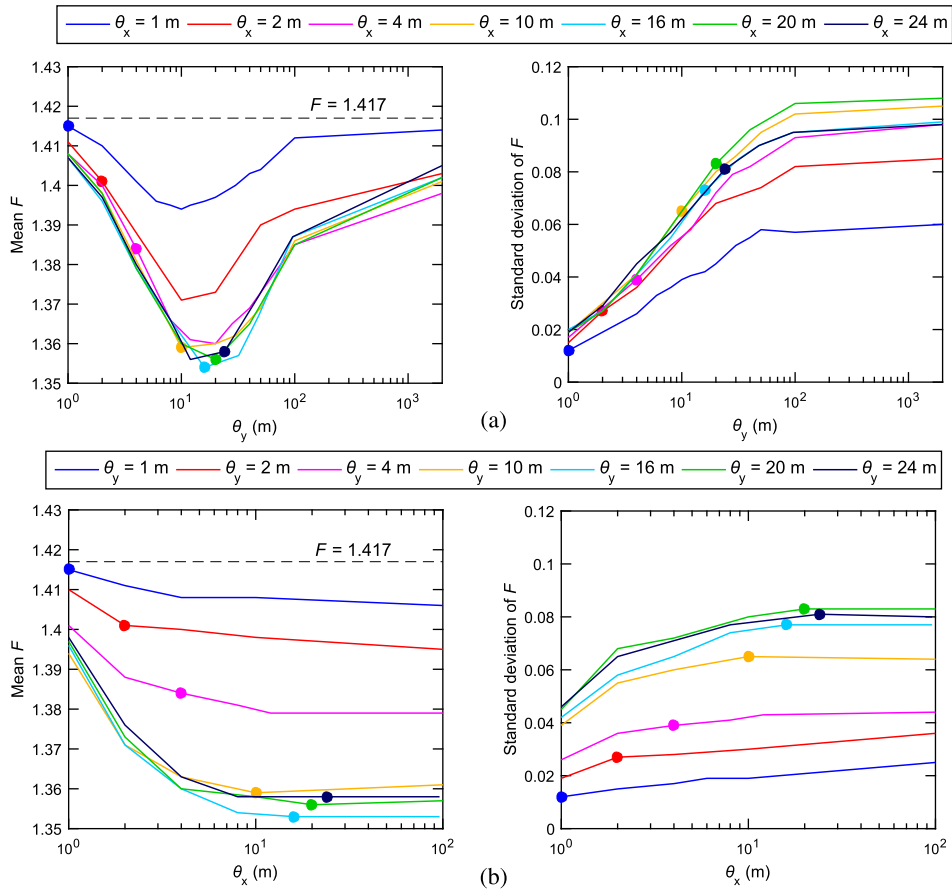


Figure 13. Mean and standard deviation of F as a function of θ_x and θ_y : (a) for fixed θ_x ; and (b) for fixed θ_y . Dashed line is the deterministic value and the filled circles are for isotropic horizontal spatial variability

4.3. Influence of 3D anisotropic material uncertainty

Varkey, Hicks, and Vardon (2017, 2019) analysed a slope with the same cross-sectional geometry and the same soil property point statistics as in this paper, but without considering a foundation layer. They observed that the results obtained by assuming isotropic spatial variability in the two horizontal directions (i.e. $\theta_h = \theta_x = \theta_y$) were consistent with the three categories of failure mode proposed by Hicks and Spencer (2010) and Hicks, Nuttall, and Chen (2014). Specifically, for a small θ_h relative to H there is much averaging of soil properties. This leads to a narrow range of solutions, a mean factor of safety that approaches the deterministic solution based on the mean soil property value, and a long (i.e. 2D) failure referred to as Mode 1. Conversely, for large values of θ_h relative to L the soil has a layered appearance. This can also lead to a long (2D) failure mechanism (Mode 3) and a mean factor of safety approaching the deterministic solution, although the range of solutions is now large because it is influenced by the relative distribution of weak and strong layers. However, Hicks and Spencer (2010)

and Hicks, Nuttall, and Chen (2014) demonstrated that Mode 2 failure was the most likely (by far) and the most critical mode of failure. This is generally associated with an intermediate value of θ_h relative to H and L , and is characterised by a discrete three-dimensional failure that tends to pass through semi-continuous weaker zones, thereby resulting in a relatively lower mean factor of safety.

Recently, a detailed investigation of the horizontal scale of fluctuation derived from CPT data, for a Dutch regional dyke (de Gast, Vardon, and Hicks 2019, 2021), has shown that the horizontal scales of fluctuation may be quite different parallel to the dyke and perpendicular to it. This may be due, for example, to the method of construction of the dyke, as well as to dykes often being located along ancient river channels, so that the correlation length along the dyke (and foundation layer) is higher than that across the dyke (i.e. $\theta_y > \theta_x$). Therefore, different scales of fluctuation in the two horizontal directions have been modelled and, due to a general lack of measured field data for horizontal correlation lengths, a wide range of values has been considered. For this investigation, only

uncertainty in the shear strength properties has been accounted for. Moreover, the slope in Figure 1 without the foundation layer has first been analysed, to enable a consistent comparison with previous findings (Hicks and Spencer 2010; Hicks, Nuttall, and Chen 2014; Hicks and Li 2018; Varkey, Hicks, and Vardon 2019).

The mean and standard deviation of F obtained for various values of the horizontal scales of fluctuation are plotted in Figure 13, and these show similar trends to those found previously when using $\theta_h = \theta_x = \theta_y$ (Hicks and Spencer 2010; Hicks, Nuttall, and Chen 2014; Varkey, Hicks, and Vardon 2019). These results have been obtained by carrying out 500 Monte Carlo realisations for each combination of θ_x and θ_y . Figure 13a shows the influence of θ_y on the computed values of F (for different values of θ_x), whereas Figure 13b shows the influence of θ_x on F (for different values of θ_y). The dashed line in the figure indicates the deterministic value of F ($= 1.417$) obtained for the slope without a foundation layer. The results obtained for isotropic horizontal spatial variability ($\theta_x = \theta_y$) in each case have been highlighted as filled circles. As shown in the figure, with an increase in the value of θ_y the range of possible solutions increases, as reflected by the higher standard deviation of F , and this increase in the range of solutions is greater than that due to a similar increase in θ_x .

Indeed, Figure 13 shows that the responses for both the mean and standard deviation of F are, in general, more influenced (with respect to the isotropic case) by a change in θ_y than a change in θ_x . Figure 13a shows that, for a given θ_x , there is a worst case θ_y with respect to the mean F , i.e. a value of θ_y for which there is a greater tendency for failure to be attracted to weaker zones, which, for this example, seems to range between approximately 10 m ($= 2H$) and 30 m ($= 6H$). Over the whole range of θ_x considered, the worst case θ_y is around 16 m (i.e. $\approx 3H$). Conversely, Figure 13b shows that, for a given θ_y , the most conservative approach is to assume a large θ_x , there not being an intermediate value of θ_x constituting a worst case. Overall, Figure 13 demonstrates that θ_y is the most influential scale of fluctuation and that, for $\theta_y > H$, it is sufficient (and generally conservative) to take $\theta_x = \theta_y$.

For very small and very large values of θ_y with respect to L , continuous long failures were observed in many realisations, corresponding to failure mode categories Mode 1 and Mode 3, respectively (Hicks and Spencer 2010; Hicks, Nuttall, and Chen 2014). In contrast, for intermediate values of θ_y , smaller discrete failures were generally observed due to failure through semi-continuous weaker zones (i.e. Mode 2 (Hicks and Spencer 2010; Hicks, Nuttall, and Chen 2014)), and

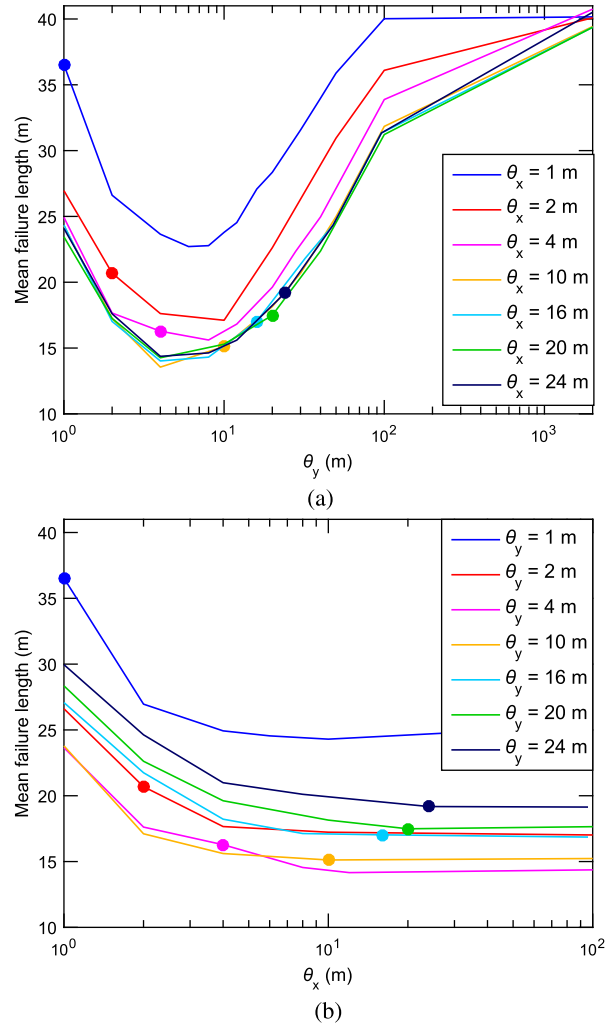


Figure 14. Mean failure lengths as a function of θ_x and θ_y : (a) for fixed θ_x ; and (b) for fixed θ_y . Filled circles are for isotropic horizontal spatial variability

sometimes multiple discrete failures, although these occurred in relatively few realisations. This is because of the relatively short length of the slope, compared to that analysed by Hicks and Li (2018), making it difficult for multiple failure mechanisms to fully develop without interaction from the mesh ends. In order to give a general impression of trends, the failure lengths in each realisation have here been calculated as the number of continuously linked elements along the slope toe having an average out-of-face displacement greater than a certain threshold value. This threshold value was calibrated using the procedure described in Hicks, Nuttall, and Chen (2014) and, for the slope analysed here, it was calibrated as 37% of the maximum out-of-face-displacement in that realisation. Although the failure lengths computed using this threshold-crossing method are only approximate, they are a good indication of trends.

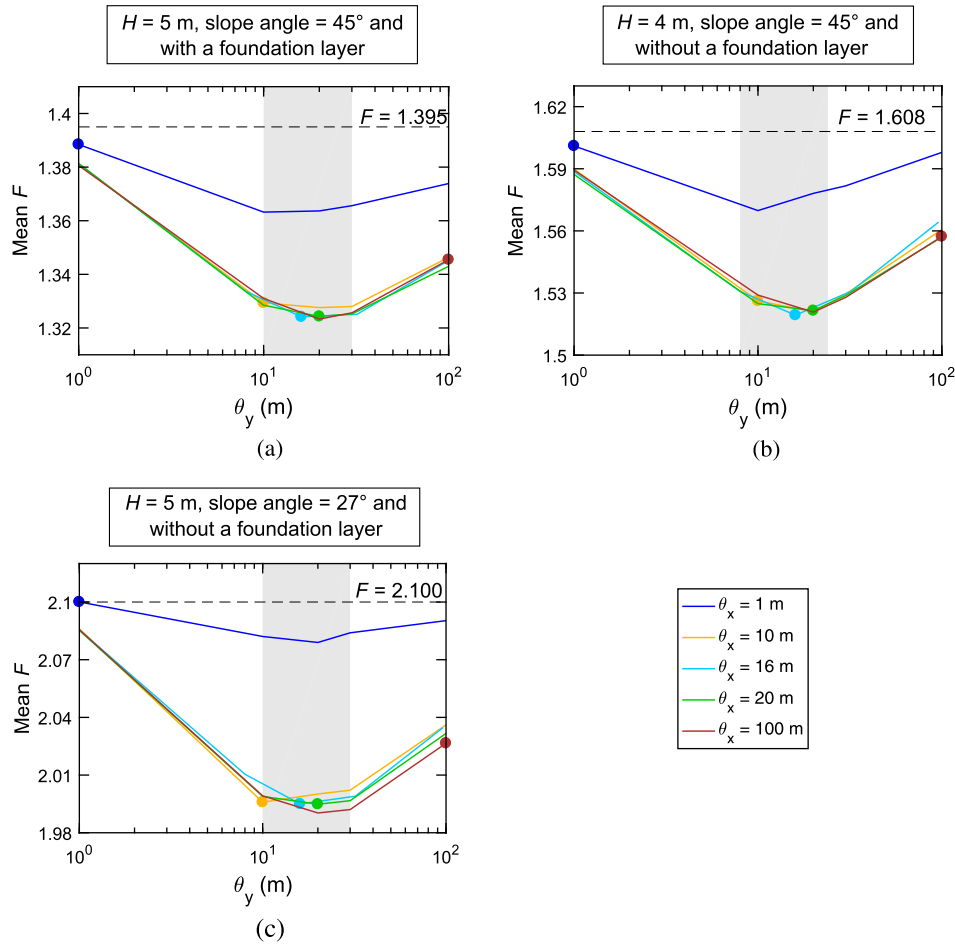


Figure 15. Mean F as a function of θ_y , obtained for: (a) slope with a foundation layer as in Figure 1; (b) and (c) slopes without a foundation layer but with a different height and slope angle, respectively. For each slope the dashed line is the deterministic F , the filled circles are for isotropic horizontal spatial variability, and the shaded grey area represents θ_y in the range $4H \pm 2H$.

The mean failure lengths obtained over all realisations for various values of θ_x and θ_y are plotted in Figure 14. The mean failure lengths for the isotropic horizontal spatial variability in each case have also been highlighted as filled circles in the figure, and are in good agreement with the relationship for the mean discrete failure length ($= 2H + \theta_h/2$) proposed by Varkey, Hicks, and Vardon (2019) (based on Hicks and Li (2018)) for intermediate values of isotropic horizontal spatial variability. Figure 14 shows that, as for the mean and standard deviation of F in Figure 13, the mean failure lengths are more influenced by a change in θ_y than a change in θ_x .

Based on the results in Figures 13 and 14, the responses obtained with anisotropic horizontal spatial variability may be significantly different compared to those based on isotropic horizontal spatial variability. However, the results suggest that it would be reasonable (and conservative) to assume isotropic spatial variability in the horizontal plane based on the value of θ_y , and that, in the absence of detailed knowledge of the site,

to assume a worst case value of θ_y . In this investigation, the worst case value of θ_y was found to be around $4H \pm 2H$.

Since this worst case value of θ_y is based on the responses obtained for slopes with the specific cross-sectional geometry shown in Figure 1, further analyses have been carried out to test the applicability of this hypothesis on a wider range of problems. In particular, three additional cases have been considered: one of the slope in Figure 1 with the foundation layer, and two cases of slopes without a foundation layer but with a different height and slope angle. These further analyses have been based on slopes that are 50 m long in the third dimension, the soil parameters listed in Table 1, a vertical scale of fluctuation of 1 m and a wide range of values of the anisotropic horizontal spatial variability. The mean values of F obtained for the various cases by carrying out 500 Monte Carlo realisations for each combination of θ_x and θ_y are plotted in Figure 15. For the various cases considered in the figure, the deterministic values of F have been shown by dashed lines and the

mean values of F obtained for isotropic horizontal spatial variability have been highlighted as filled circles. The figure demonstrates (once again) the significant influence of θ_y on the responses and that, for $H < \theta_y \ll L$, it may be sufficient to assume $\theta_x = \theta_y$. The results also indicate that in the absence of a detailed site investigation, it may be reasonably conservative to assume isotropic spatial variability in the horizontal plane based on a worst case value of θ_y , which falls well within the range $\theta_y = 4H \pm 2H$ indicated by shaded grey area in Figure 15.

5. Conclusions

RFEM has been used to study the influence of three forms of uncertainty on the probabilistic characteristics of the stability of an idealised 3D embankment slope: these were due to 1D spatial variability in the external geometry of the slope along its length, 2D spatial variability in the depth of the boundary between the embankment material and the foundation layer, and 3D spatial variability in the shear strength properties of the slope and foundation materials. The uncertainties in external geometry were modelled as variations in the slope height, crest width and toe width along the slope length.

It was observed that uncertainties relating to the external geometry and inter-layer boundary had little to negligible influence on the probabilistic characteristics of the slope stability compared to spatial variability in the shear strength properties of the slope and foundation materials, based on typical statistics for a Dutch regional dyke. It was also observed that the resulting distribution of the factor of safety F considering the geometric or inter-layer boundary uncertainty was centred near the deterministic F based on the mean parameter values, whereas it was centred at a smaller value of F when uncertainty in the material properties was included due to the presence of weaker zones attracting failure. Additional analyses carried out with different slope geometries and with different strength parameters for the foundation material further demonstrated the significant influence of the material characteristics and the negligible influence of inter-layer boundary uncertainty on the slope response.

It was demonstrated that anisotropy of soil spatial variability in the horizontal plane can have a significant influence on embankment reliability and failure consequence, with the spatial correlation of properties along the embankment length (θ_y) having a much greater influence than the spatial correlation of properties perpendicular to it (θ_x). Furthermore, for very small and very large values of θ_y relative to the embankment length, continuous long failures were observed, whereas

for intermediate values of θ_y , smaller discrete failures were generally observed due to failure through semi-continuous weaker zones.

The results indicated that assuming isotropic spatial variability in the horizontal plane could give either conservative or unconservative solutions. However, a conservative solution is generally obtained by assuming isotropic variability based only on the scale of fluctuation along the embankment. For those cases in which an accurate knowledge of θ_y is not available, a worst case value of $\theta_y \approx 4H \pm 2H$ was found for the range of embankments analysed.

Acknowledgements

This work is part of the research programme Reliable Dykes with project number 13864 which is financed by the Netherlands Organisation for Scientific Research (NWO), and was carried out on the Dutch National e-infrastructure with the support of SURF Foundation.

Disclosure statement

No potential conflict of interest was reported by the authors.

ORCID

Michael A. Hicks  <http://orcid.org/0000-0002-7603-7040>

References

- Cherubini, C. 2000. "Reliability Evaluation of Shallow Foundation Bearing Capacity on $c' \phi'$ Soils." *Canadian Geotechnical Journal* 37: 264–269.
- Ching, J., T. J. Wu, A. W. Stuedlein, and T. Bong. 2018. "Estimating Horizontal Scale of Fluctuation with Limited CPT Soundings." *Geoscience Frontiers* 9 (6): 1597–1608.
- de Gast, T. 2020. *Dykes and Embankments: A Geostatistical Analysis on Soft Terrain. Dissertation*. Delft University of Technology, The Netherlands.
- de Gast, T., M. A. Hicks, A. P. van den Eijnden, and P. J. Vardon. 2021. "On the Reliability Assessment of a Controlled Dyke Failure." *Géotechnique* 71 (11): 1028–1043.
- de Gast, T., P. J. Vardon, and M. A. Hicks. 2019. "Observations and Considerations Regarding Estimating Horizontal Scales of Fluctuation Around Linear Infrastructure." In *Proceedings of 7th International Symposium on Geotechnical Safety and Risk*, edited by J. Ching, D. Q. Li, and J. Zhang, 340–345. Taipei, Taiwan: Research Publishing.
- de Gast, T., P. J. Vardon, and M. A. Hicks. 2021. "Assessment of Soil Spatial Variability for Linear Infrastructure Using Cone Penetration Tests." *Géotechnique* 71 (11): 999–1013.
- Deng, Z. P., D. Q. Li, X. H. Qi, Z. J. Cao, and K. K. Phoon. 2017. "Reliability Evaluation of Slope Considering Geological Uncertainty and Inherent Variability of Soil Parameters." *Computers and Geotechnics* 92: 121–131.

- El-Ramly, H., N. R. Morgenstern, and D. M. Cruden. 2003. "Probabilistic Stability Analysis of a Tailings Dyke on Presheared Clay-Shale." *Canadian Geotechnical Journal* 40: 192–208.
- Elfeki, A., and M. Dekking. 2001. "A Markov Chain Model for Subsurface Characterization: Theory and Applications." *Mathematical Geology* 33: 569–589.
- Fenton, G. A., and D. V. Griffiths. 2008. *Risk Assessment in Geotechnical Engineering*. New York: Wiley.
- Fenton, G. A., and E. H. Vanmarcke. 1990. "Simulation of Random Fields via Local Average Subdivision." *Journal of Engineering Mechanics* 116: 1733–1749.
- Griffiths, D. V., and G. A. Fenton. 2004. "Probabilistic Slope Stability Analysis by Finite Elements." *Journal of Geotechnical and Geoenvironmental Engineering* 130 (5): 507–518.
- Griffiths, D. V., J. Huang, and G. A. Fenton. 2009a. "Influence of Spatial Variability on Slope Reliability Using 2-D Random Fields." *Journal of Geotechnical and Geoenvironmental Engineering* 135 (10): 1367–1378.
- Griffiths, D. V., J. Huang, and G. A. Fenton. 2009b. "On the reliability of earth slopes in three dimensions." *Proceedings of the Royal Society - A: Mathematical, Physical and Engineering Sciences* 465 (2110): 3145–3164.
- Hicks, M. A., and Y. Li. 2018. "Influence of Length Effect on Embankment Slope Reliability in 3D." *International Journal for Numerical and Analytical Methods in Geomechanics* 42: 891–915.
- Hicks, M. A., J. D. Nuttall, and J. Chen. 2014. "Influence of Heterogeneity on 3D Slope Reliability and Failure Consequence." *Computers and Geotechnics* 61: 198–208.
- Hicks, M. A., and C. Onisiphrou. 2005. "Stochastic Evaluation of Static Liquefaction in a Predominantly Dilative Sand Fill." *Géotechnique* 55: 123–133.
- Hicks, M. A., and K. Samy. 2002. "Influence of Heterogeneity on Undrained Clay Slope Stability." *Quarterly Journal of Engineering Geology and Hydrogeology* 35 (1): 41–49.
- Hicks, M. A., and K. Samy. 2004. "Stochastic Evaluation of Heterogeneous Slope Stability." *Italian Geotechnical Journal* 38 (2): 54–66.
- Hicks, M. A., and W. A. Spencer. 2010. "Influence of Heterogeneity on the Reliability and Failure of a Long 3D Slope." *Computers and Geotechnics* 37: 948–955.
- Hicks, M. A., D. Varkey, A. P. van den Eijnden, T. de Gast, and P. J. Vardon. 2019. "On Characteristic Values and the Reliability-Based Assessment of Dykes." *Georisk: Assessment and Management of Risk for Engineered Systems and Geohazards* 13: 313–319.
- Huang, J., D. V. Griffiths, and G. A. Fenton. 2010. "System Reliability of Slopes by RFEM." *Soils and Foundations* 50 (3): 343–353.
- Huang, J., A. V. Lyamin, D. V. Griffiths, K. Krabbenhoft, and S. W. Sloan. 2013. "Quantitative Risk Assessment of Landslide by Limit Analysis and Random Fields." *Computers and Geotechnics* 53: 60–67.
- Javankhoshdel, S., N. Luo, and R. J. Bathurst. 2017. "Probabilistic Analysis of Simple Slopes with Cohesive Soil Strength using RLEM and RFEM." *Georisk: Assessment and Management of Risk for Engineered Systems and Geohazards* 11 (3): 231–246.
- Ji, J., and C. L. Chan. 2014. "Long Embankment Failure Accounting for Longitudinal Spatial Variation - A Probabilistic Study." *Computers and Geotechnics* 61: 50–56.
- Johari, A., and M. Gholampour. 2018. "A Practical Approach for Reliability Analysis of Unsaturated Slope by Conditional Random Finite Element Method." *Computers and Geotechnics* 102: 79–91.
- Juang, C. H., J. Zhang, M. Shen, and J. Hu. 2019. "Probabilistic Methods for Unified Treatment of Geotechnical and Geological Uncertainties in a Geotechnical Analysis." *Engineering Geology* 249: 148–161.
- Li, Y. 2017. *Reliability of Long Heterogeneous Slopes in 3D. Dissertation*. Delft University of Technology, The Netherlands.
- Li, Y., M. A. Hicks, and J. D. Nuttall. 2015. "Comparative Analyses of Slope Reliability in 3D." *Engineering Geology* 196: 12–23.
- Li, Z., X. Wang, H. Wang, and R. Y. Liang. 2016. "Quantifying Stratigraphic Uncertainties by Stochastic Simulation Techniques Based on Markov Random Field." *Engineering Geology* 201: 106–122.
- Li, X. Y., L. M. Zhang, and J. H. Li. 2016. "Using Conditioned Random Field to Characterize the Variability of Geologic Profiles." *Journal of Geotechnical and Geoenvironmental Engineering* 142 (4): 04015096.
- Liang, Y. R., Z. Z. Wang, and J. H. Guo. 2014. "Reservoir Lithology Stochastic Simulation Based on Markov Random Fields." *Journal of Central South University* 21: 3610–3616.
- Lloret-Cabot, M., G. A. Fenton, and M. A. Hicks. 2014. "On the Estimation of Scale of Fluctuation in Geostatistics." *Georisk: Assessment and Management of Risk for Engineered Systems and Geohazards* 8 (2): 129–140.
- Phoon, K. K., and F. H. Kulhawy. 1999. "Characterization of Geotechnical Variability." *Canadian Geotechnical Journal* 36: 612–624.
- Qi, X. H., D. Q. Li, K. K. Phoon, Z. J. Cio, and X. S. Tang. 2016. "Simulation of Geologic Uncertainty Using Coupled Markov Chain." *Engineering Geology* 207: 129–140.
- Rackwitz, R. 2000. "Reviewing Probabilistic Soils Modelling." *Computers and Geotechnics* 26: 199–223.
- Spencer, W. A. 2007. *Parallel Stochastic and Finite Element Modelling of Clay Slope Stability in 3D. Dissertation*. University of Manchester, UK.
- van den Eijnden, A. P., and M. A. Hicks. 2017. "Efficient Subset Simulation for Evaluating the Modes of Improbable Slope Failure." *Computers and Geotechnics* 88: 267–280.
- Vardon, P. J., K. Liu, and M. A. Hicks. 2016. "Reduction of Slope Stability Uncertainty Based on Hydraulic Measurement via Inverse Analysis." *Georisk: Assessment and Management of Risk for Engineered Systems and Geohazards* 10 (3): 223–240.
- Varkey, D., M. A. Hicks, A. P. van den Eijnden, and P. J. Vardon. 2020. "On Characteristic Values for Calculating Factors of Safety for Dyke Stability." *Géotechnique Letters* 10: 353–359.
- Varkey, D., M. A. Hicks, and P. J. Vardon. 2017. "Influence of Spatial Variability of Shear Strength Parameters on 3D Slope Reliability and Comparison of Analysis Methods." In *Proceedings of 6th International Symposium on Geotechnical Safety and Risk*, 400–409. Colorado, USA.
- Varkey, D., M. A. Hicks, and P. J. Vardon. 2019. "An Improved Semi-Analytical Method for 3D Slope Reliability Assessments." *Computers and Geotechnics* 111: 181–190.

- Wang, X., H. Wang, R. Y. Liang, and Y. Liu. 2019. "A Semi-Supervised Clustering-Based Approach for Stratification Identification Using Borehole and Cone Penetration Test Data." *Engineering Geology* 248: 102–116.
- Xiao, T., L. M. Zhang, X. Y. Li, and D. Q. Li. 2017. "Probabilistic Stratification Modelling in Geotechnical Site Characterization." *ASCE-ASME Journal of Risk and Uncertainty in Engineering Systems, Part A: Civil Engineering* 3 (4): 04017019.
- Zhao, T., and Y. Wang. 2020. "Interpolation and Stratification of Multilayer Soil Property Profile from Sparse Measurements Using Machine Learning Methods." *Engineering Geology* 265: 105430.